



Wear mechanisms in microfabricated ball bearing systems



Brendan Hanrahan^{a,b}, Saswat Misra^c, C. Mike Waits^d, Reza Ghodssi^{c,*}

^a Formerly Materials Science and Engineering Department, University of Maryland, College Park, MD 20704, USA

^b Currently Oak Ridge Associated Universities Fellowship Program, U.S. Army Research Laboratory, 2800 Powder Mill Road, Adelphi, MD 20783, USA

^c Electrical and Computer Engineering Department, Institute for Systems Research, University of Maryland, 2173 A.V. Williams Building, College Park, MD 20704, USA

^d U.S. Army Research Laboratory, 2800 Powder Mill Road, Adelphi, MD 20783, USA

ARTICLE INFO

Article history:

Received 3 September 2014

Received in revised form

20 December 2014

Accepted 22 December 2014

Available online 31 December 2014

Keywords:

Rolling friction

Micro-abrasion

Galling

Bearings

Surface analysis

ABSTRACT

Microfabricated ball bearings have been demonstrated successfully in a number of microsystems, although a complete understanding of their tribological properties remains elusive. This paper investigates the wear mechanisms for a microfabricated ball bearing platform that includes silicon and thin-film coated silicon raceway/steel ball materials systems. Adhesion of ball material, found to be the primary wear mechanism, is universally present in all tested materials systems. Volumetric adhesive wear rates are observed between 4×10^{-4} and $4 \times 10^{-5} \mu\text{m}^3/\text{mN} \cdot \text{rev}$. Pressured-induced phase changes take place in the contact areas of the bare silicon raceways, observed with Raman spectroscopy. An understanding of the wear mechanisms within microfabricated ball bearings will help optimize operational parameters and materials systems for long-term reliability.

© 2015 Elsevier B.V. All rights reserved.

1. Introduction

Rolling bearings are universally employed in macroscale machinery to provide a low friction and wear contact for fast moving, loaded components. Recently, rolling bearing technology has been extended to the realm of micro-electromechanical systems (MEMS) in the demonstration of high-performance linear and rotary micromachines. The microscale rolling bearings differ from macro bearings in both materials systems due to the use of silicon-based microfabrication technology versus steel machining and size scales with feature sizes on the order of 100s of micrometers versus centimeters to meters. The understanding of wear mechanisms specific to rolling bearing microsystems materials and geometries will ultimately enable the long-term use of high-performance micromachinery.

Microfabricated ball bearing systems provide long travel, minimal friction and wear, and good mechanical stability. Linear and rotary micromachines are attractive for power, sensing, and actuation applications, such as micropumps [1], microgenerators [2], and micromotors [3–5]. Friction within the microball bearings has been modeled in [6] and experimentally explored in [7–12].

The wear mechanisms present in microfabricated systems differ significantly from macroscale counterparts, and therefore, need to be specifically addressed. This difference is due to (1) the increased

surface-to-volume ratio obtained from scaling features to shorter length scales, enhancing the influence adhesion; and (2) the specific materials systems used in integrated circuit microfabrication techniques, which are often times non-ideal for mechanical/tribological applications. Wear studies within the MEMS domain are typically split into two experimental categories [13]: *in situ* testing [11,14,15], in which wear is qualitatively described by observation or characterized by a number of cycles or device lifetime [10]; and tribometer-based studies [16–18], where contact is initiated in a pin-on-disc methodology using MEMS materials of interest. A classic example of *in situ* wear testing of micromachined silicon structures was performed by Mehregany et al., where the authors fabricated a side-drive polysilicon wobble motor [19]. Motor rotational speed is a function of the gap between rotor and stator, which changes gradually with the wear of the contact bearing. The authors determined that there were three primary regimes of operation for such a device: the burn-in period, where large asperities on the bearing from the reactive ion etching are smoothed; the break-in period, where the speed of the motor gradually increases from smoothing of the surface roughness; and the rotor slip region, where the rotor speed departs from the exciting voltage due to slip. Tambe et al. published a study that highlighted the scale and material dependence of tribological phenomena using a micro-tribometer for the microscale portion and a modified atomic force microscope (AFM) for the nanoscale study [20]. In this study, the adhesive force between contacting materials showed a strong dependence on residence time, humidity, and temperature, which can be related to water vapor-derived meniscus forces developed between

* Corresponding author. Tel.: +1 301 405 8158.

E-mail address: ghodssi@umd.edu (R. Ghodssi).

the contact point and substrate. Additionally, a velocity dependence on friction force was discovered for multiple material systems, further strengthening the argument that tribological phenomena are strongly scale dependent. Ku et al. bridged the gap between *in situ* testing and a tribometer by fabricating silicon thrust contact bearing geometries to act as the pin of the pin-on-disc methodology [21]. The authors found a significant dependence on surface state of the measured coefficient of friction and wear rates. This result was deduced from a comparison of samples tested immediately after oxygen plasma cleaning and samples left out in “room air” for a period of 15 h. A majority of these studies are focused on sliding regime wear mechanisms on micro-to-nano length scales, with little focus on the unique realm of microscale rolling contact.

Thin-film coatings are capable of greatly affecting the tribological properties of a system owing to the fact that friction and wear phenomena generally initiate at the surface or near-surface of contacting bodies. Two regimes exist for the use of solid thin films in a tribological system: those that act as lubrication and wear in a manner that reduces friction, e.g., graphite [22] or molybdenum disulfide [23]; and those that remain intact and reduce the chemical affinity for the contacting surfaces or enhance the mechanical properties of the surfaces. Solid film lubricants are typically used in situations where it is difficult to maintain a fluid film boundary layer, such as high load or high speed operation. Hard thin films are used in applications where debris generation is not tolerable. In the current demonstration of microball bearings, hard film coatings are employed to alter the surface mechanical and chemical properties in an attempt to enhance the tribology of the overall system. Silicon carbide (SiC) thin-film coatings were shown to improve the performance of a microfabricated ball bearing by reducing the coefficient of friction (COF) from 0.002 to 0.0006 over bare silicon raceways [8]. At high loads (10–500 mN), fracture was observed for similar SiC coated raceways, while ultrananocrystalline diamond (UNCD) films exhibited virtually no wear over the same range of loads [9]. Bandorf et al. used a number of carbon-based thin films to minimize wear and friction coefficient. This work found that the influence of the mechanical properties of the substrate played a significant role in reducing wear depth in tape-abrasive testing, increasing the tape length (lifetime) to obtain a given wear depth by almost an order of magnitude by using a polymer substrate versus silicon [24]. It was also found that increasing film hardness improved the tribological properties of the system. In summary, a majority of the microscale wear studies described above have highlighted the importance of both substrate and thin-film materials properties regarding wear.

This work explores the wear mechanisms that dictate the performance of the microfabricated encapsulated ball bearing within the platform of a microturbine. Worn raceways are dissected and the wear mechanisms are studied using Raman spectroscopy and electron dispersive X-ray spectroscopy (EDS) in conjunction with scanning electron microscopy (SEM), and optical profilometry. The friction torque, which is indicative of wear, is evaluated using spin-down deceleration through successive levels of run-in wear. These tests and analysis methods were carried out on bare silicon raceways, as well as raceways coated with SiC and titanium nitride (TiN) hard thin films. Certain load and material combinations will result in a specific wear mechanism. An understanding of such mechanisms will allow the design of engineering systems with minimum wear and maximum lifetimes.

2. Materials and methods

2.1. Microturbine Platform

A silicon microturbine was chosen as the experimental platform for this study. This device has been previously described in a number

of publications [11,25]. A schematic of the microtribology device (MTD) with 100 285- μm -diameter 440C stainless steel balls is shown in Fig. 1.

The MTD was selected because it can perform normal-load-resolved friction testing, and has a high fabrication yield and consistent surface quality within the races. As shown in [3], the encapsulated bearings can be integrated into integrated circuit fabrication flows to create future motors, generators, and sensors.

Packaging of the MTD allows for independent turbine and thrust flow while simultaneously measuring the speed via an optical displacement sensor (ODS) on etched equiradial tracking marks, the turbine input pressure and flow rate, and the thrust plenum pressure. The thrust plenum, created by an o-ring sealed cavity between the device and packaging, allows for variable normal loads to be acted on the rotor independent of speed.

The MTD rotor is fabricated using two silicon wafers containing a shallow and deep-etched race half to achieve an offset bearing-bond interface, with a third wafer comprising the air manifold layer (Fig. 1). The offset bond interface is used to prevent ball contact on the corners of the bonded wafers. To obtain offset interfaces and alignment pits simultaneously, an asymmetrical etching scheme is employed, described thoroughly in [26]. The dimensions of a completed bearing are presented in Fig. 2.

The bearing surfaces have been characterized to assure consistency among the tested devices. The roughness of the raceway is RMS 5 nm. There is a slight radius to the bottom of the raceway, a typical product of the etch process. For first approximations of contact mechanics, the raceway is assumed to be flat. The sidewall roughness is a function of the ratio of etching to deposition time in the deep reactive-ion etching (DRIE) process, found to be 160-nm scallops. Ideally, the balls will not contact the sidewall because the frictional force will keep them in place. Realistically, the balls are not all under equal load due to waviness in the raceway from the etch process; therefore, there is intermittent contact with the sidewall. The sidewall wear is characterized below.

2.2. Wear testing

Seven microturbines were used to determine the wear mechanisms within the microfabricated ball bearing systems: five turbines with bare silicon raceways and two turbines with hard film coatings. The testing conditions and ultimate failure mechanisms are summarized in Table 1.

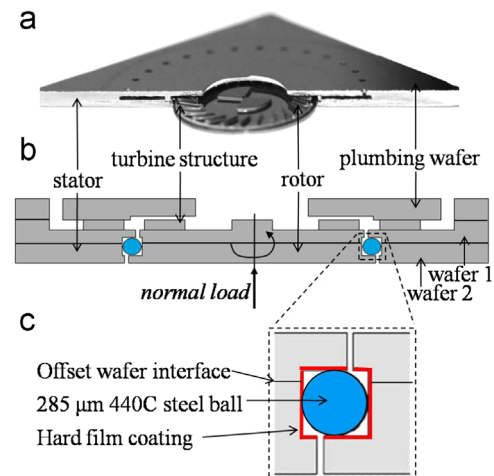


Fig. 1. (a) Photograph of the cross-sectioned MTD stator with a rotor inserted. (b) Cross-sectional schematic of the device showing a rotor, stator, and the bonded wafers that create the offset bearing interface, and (c) detail of the bearing.

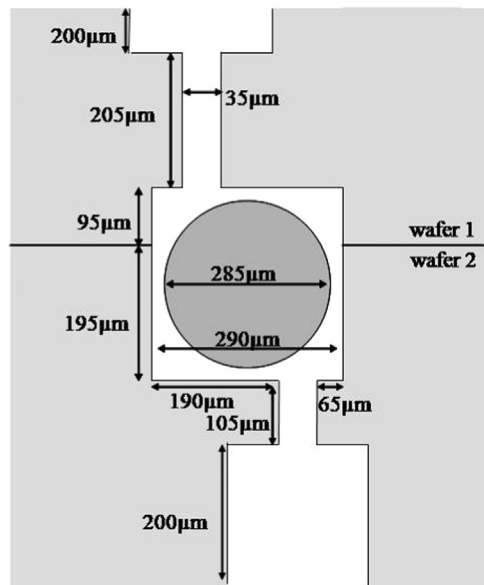


Fig. 2. Dimensioned schematic of the ball bearing in the housing.

Table 1

Summary of the experimental conditions of the accelerated wear test silicon raceways.

Device	Rotor load	Device lifetime	Stress/ball (MPa)	Coating	Failure mechanism
D1	10 mN	2 Mrev	142	n/a	inspection
D2	10 mN	2 Mrev	140	TiN	spalling
D3	10 mN	2 Krev	129	SiC	coating fracture
D4	50 mN	3 Mrev	242	n/a	fabrication defect
D5	100 mN	205 Mrev	306	n/a	n/a
D6	200 mN	20 Mrev	385	n/a	inspection
D7	400 mN	400 Krev	485	n/a	raceway fracture

Wear of the silicon raceway was induced through a series of accelerated wear tests. To perform these tests, the compressed gas is used to impart 10 to 400 mN normal loads on the rotor while the device is actuated at speeds of 6000–12,000 rpm by gas flow through turbine actuation structures. These speeds are chosen for wear testing to minimize the effect of centripetal acceleration of the balls, addressing the effect of load dependence on the wear rate of the turbines ideally operating as thrust bearings (ball axis of rotation perpendicular to rotor axis of rotation). After successive operation cycles, the microturbine performance is evaluated by plotting speed versus input power, as described in the section below (Fig. 3). Devices were disassembled at different intervals and the wear was measured geometrically with optical profilometry (Veeco WYKO NT 1100), and visually with SEM and optical microscopy.

2.3. Hard film coating

TiN and SiC thin films were chosen because of their high hardness and their compatibility with microfabrication techniques. SiC and TiN films were sputtered onto a bare silicon substrate after successive O₂ plasma and Ar plasma cleaning steps. The SiC films were sputtered in an AJA ATV 1800-V sputtering tool to a thickness of 250 nm from a SiC target in an argon atmosphere. The chamber pressure is held at 2.5 mTorr and the DC sputtering source is operated at 1 kW without any external substrate heating. It is assumed that these conditions produce an amorphous film, supported in [27].

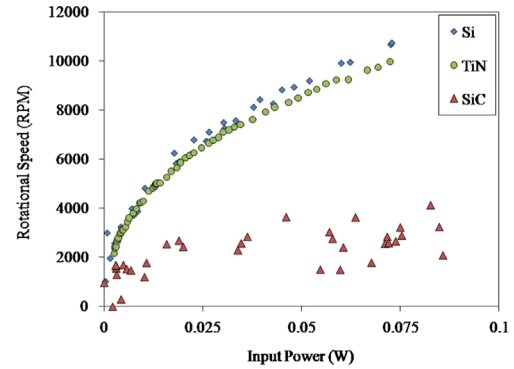


Fig. 3. Performance curves taken from virgin raceways coated with SiC, TiN thin films or left bare. SiC films erratic behavior is due to significant wear.

Table 2

Mechanical properties of thin-film/Si systems probed via nanoindentation.

	Bare Si	250 nm TiN	250 nm SiC
Stiffness (GPa)	169	155.9	127.1
Hardness (GPa)	13.4	15.7	17.7

TiN films were deposited in a reactive sputtering process in a CVC 610 sputtering tool. First, a thin Ti adhesion layer was deposited at 5 mTorr, and 1 kW, in an argon environment. Next, TiN was sputtered from a Ti target in a N₂ plasma at 2–5 mTorr and 1 kW after a 30 min pre-sputter that nitrates the surface of the target. Reactively sputtered TiN is typically stoichiometric and has a columnar grain structure [28]. The total film thickness of the Ti/TiN stack is 250 nm. The mechanical properties of these films have been explored by nanoindentation methods and are summarized in Table 2.

3. Results and discussion

3.1. Microturbine Performance

Microturbine performance is used to measure the general efficiency of the turbine, which is directly related to the condition of the raceways. Etched silicon races, coated with TiN or SiC thin films, and raceways left uncoated were evaluated. The two mechanical properties of interest, hardness and stiffness, of these films is reported in Table 2.

Reduced mechanical deformation from increased hardness could reduce friction and wear by two mechanisms: reducing the amount of energy lost to plastic deformation and reducing the area of contact between the ball and raceway. Initial characterization of the coated raceways within a MTD was done using the speed versus input power performance testing method described above. During this test, the rotor is imparted a normal force of up to 12 mN from the pressurization of the thrust cavity due to turbine pressure leaking through the bearings. This relatively low load proved enough to start rapidly wearing the SiC film while the TiN coated and bare Si raceways performed nearly identically. The results from the initial performance characterization, including the wearing of the SiC thin film, can be indirectly observed in Fig. 3 by the low speeds obtained at high input power. The accelerated wear of the SiC film is discussed in the following section.

A performance assessment of the bare silicon turbine is performed with and without cleaning beyond 55 million revolutions (M rev.) to better understand the long-term wear mechanisms. Fig. 4 highlights two aspects of the long-term turbine performance.

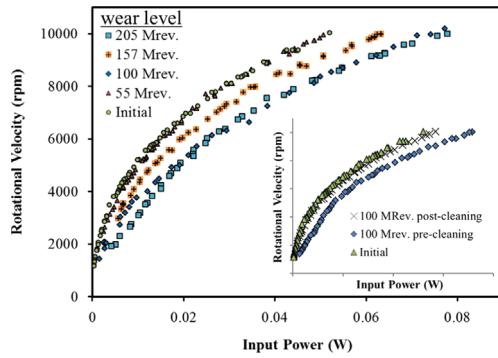


Fig. 4. Performance curves for a single MTD through progressive levels of wear. (Inset) Performance characterization of the MTD before and after cleaning at 100M rev. wear level, compared to initial values.

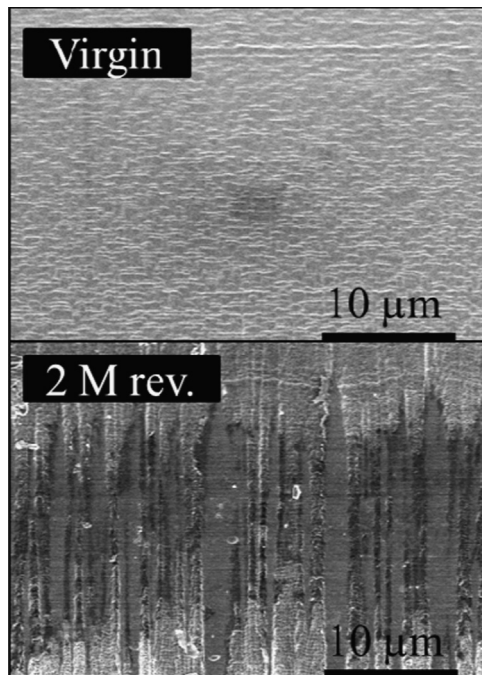


Fig. 5. SEM images of the sidewalls before testing and after 2M rev. at an average of 10,000 rpm.

The MTD performance is measured initially and then at progressive levels of wear up to 205M rev., measured before cleaning. The inset graph compares the performance before and after cleaning to the initial performance for a representative level of wear. In between performance characterizations, the device is run at 100-mN normal load to accelerate the wear process.

The MTD performance is shown to degrade between the 55M and 205M rev. test, in that it takes up to 75% more power to reach a given turbine speed. The observed performance degradation is most likely due to the random ejection and build-up of sidewall material from ball-sidewall impacts during operation. Fig. 4 (inset) shows the performance curve at the 100 M rev. level directly after testing (pre-cleaning) and after cleaning procedure, revealing that the turbine performance improves after cleaning. Fig. 5 compares the sidewalls of virgin and tested devices after 2 M rev.

Ejected wear debris was observed on the plumbing wafer in tests that spanned 5M rev. or more. Fig. 6(a) shows the plumbing wafer removed from the MTD package after 45M rev. operation. A halo of wear debris, following the blade arrangement of the turbine can be observed around the turbine outlet. Fig. 6(b) and (c) shows

the SEM micrographs of the wear debris and the subsequent EDS chemical analysis clearly showing the wear debris is composed primarily of iron and therefore originates from the microball.

Figs. 5 and 6 exhibit the two debris-generating mechanisms during long-term turbine operation. This debris can be removed by ultrasonic cleaning of the device, which is shown Fig. 4 (inset), where the device returned to original performance values after a cleaning procedure. The ratio of the effects side wall (silicon) to ball (steel) debris is not known, although the steel debris is significantly more numerous after testing.

Spin-down friction testing was used in conjunction with the turbine performance testing to compare the TiN and bare-Si raceway friction. The spin-down test procedure is described in [10]. TiN raceways were tested to the same rotor load/revolution metric as a bare silicon turbine (10 mN/2M rev.). The initial values of dynamic friction torque (DFT) were similar for TiN and Si raceways, as seen in Fig. 7a.

Despite having a higher hardness, there was no observed reduction in friction in the initial test. This could be due to the enhanced influence of surface properties over volumetric properties, as is the case in systems with reduced geometries.

Following the initial test, the TiN-coated and Si MTD were run at 10-mN rotor normal loads for 1M rev. and then re-tested. This process was repeated twice. Fig. 7b compares the DFT values of the Si and TiN coated raceways after 2M rev. wear. It can be observed that the Si raceway maintains consistent performance while the TiN coated raceway becomes increasingly more erratic. DFT testing was not performed beyond 2M rev. so that the raceways could be inspected, a destructive process for the microturbine.

3.2. Wear mechanisms

3.2.1. Pressure-induced silicon phase change

Fig. 8 shows Raman spectra comparing worn and unworn regions of two silicon raceways (D1 and the microturbine in [1]). The broad peak at 160 cm^{-1} and the shoulder at 470 cm^{-1} coincide with a stress-induced amorphous-silicon (α -Si) phase specific to the worn areas of the race.

Previous work on the characterization of nanoindentation of silicon with spherical indenters acts as a close analog to the morphologies observed in the microball bearing. The results presented in [29,30] show that pressure-induced phase transformations occur at contact pressures on the order of 2 GPa up to 7 GPa, which is an order of magnitude higher than the calculated contact pressure for the microball bearings tested. In our devices, the phase change is observed at 140 and 500 MPa average ball stresses, assuming 100 balls are equally supporting the load, for rotor loads of 10 and 500 mN, suggesting that either peak stress within the turbine is much higher than calculations or the phase change mechanism is rate dependent. The calculated peak stress is known to be an underestimate of the actual peak stress due to the assumption that all balls are in contact with the raceway uniformly. Realistically, a fraction of balls are supporting the rotor normal load due to the raceway waviness, and therefore, the actual peak loads are much higher. The nanoindentation studies also showed other silicon crystalline phases present in the solid after indentation whose amount and morphology were highly dependent on the kinetics of the loading procedure [31]. The lack of alternative Si phases in our work could be due to the cyclical nature of the loading and the short elastic recovery time between loadings or below the amount of phases could be below the resolution of our testing methodology. α -Si has a reported Young's modulus and hardness of up to 80% and 90% of that of single crystalline Si [32], and up to a 67% increased fracture toughness [33]. The slightly reduced modulus and hardness would cause, if anything, slightly higher rolling friction due to increased deformation (elastic and plastic), although some overall benefit may

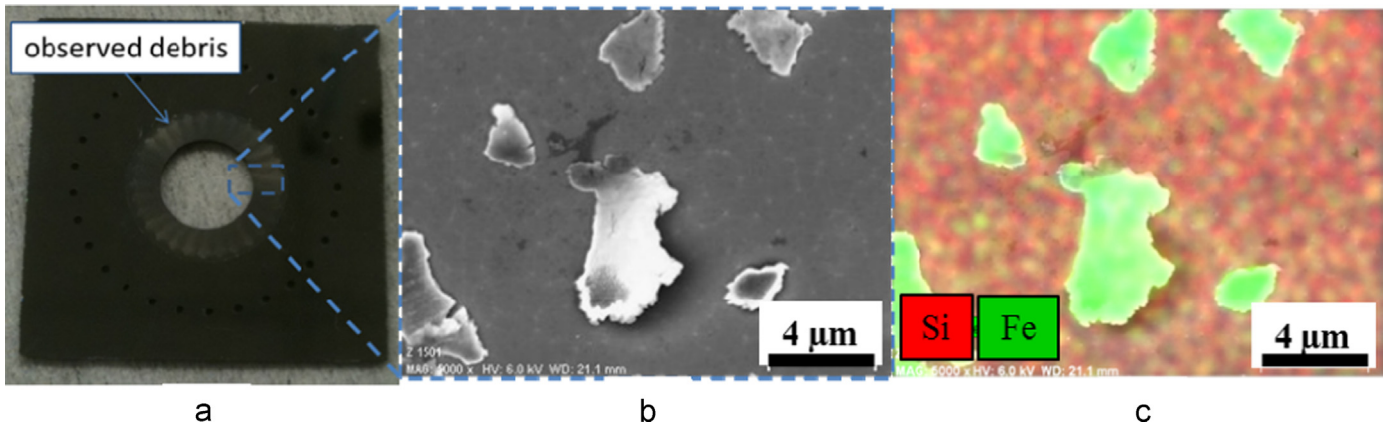


Fig. 6. (a) Optical image of the plumbing wafer after 45M rev. testing, (b) SEM image of the ejected wear debris and (c) chemical analysis of the SEM image showing the ejected debris is ball material.

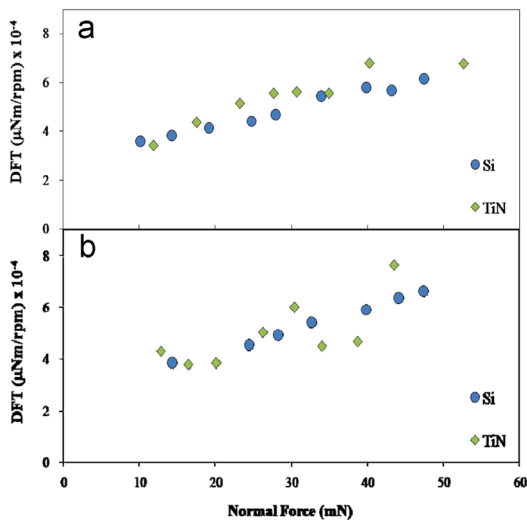


Fig. 7. (a) DFT values for bare Si and TiN coated systems. Both systems follow the linear relationship between DFT and normal load. (b) DFT values for raceways after 2M rev. of run-in. Si raceways remain consistent, while the TiN coated systems begin to exhibit erratic behavior. Figure reproduced from [9].

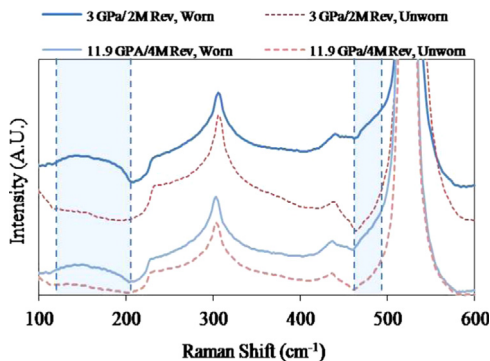


Fig. 8. Raman spectra from two silicon raceways, tested to a maximum contact stress of 3 and 11.9 GPa. Amorphous silicon phase present in worn areas, at 160 and 470 cm^{-1} and not visible in unworn areas of the same bearing.

be realized because of the reduction in wear rates due to the increased fracture toughness of the a-Si; therefore, the net performance benefit/detriment is unknown.

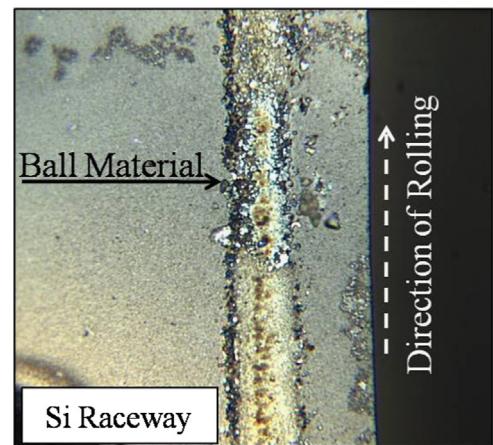


Fig. 9. Optical micrograph of silicon raceway after 2M rev. wear. Stainless steel ball material can be observed throughout, in both trace amounts and significant islands.

3.2.2. Ball material adhesion

The primary mechanism of wear observed in the tested micro-systems is of an adhesive nature between the ball and the raceway. This mechanism is also linked to the observed friction within the microfabricated ball bearings [12]. Fig. 9 shows an optical micrograph from D1 showing patches of ball material adhered to the silicon raceway.

The adhesion mechanism is described schematically in Fig. 10. Adhesion occurs when contacting materials are placed under high pressures. During rolling, temporary bonds are made between the ball and the raceway. As the ball continues to roll, shear stress acts to create a surface with minimum energy, on some occasions shearing through the ball instead of the ball/raceway interface, leaving adhered ball material behind.

Optical profilometry was used to determine the geometry of the adhered ball material. A characteristic profile of the adhered wear debris is shown in Fig. 11, from device D6 operated at 200-mN rotor load for 20 M rev. The average height of wear debris was measured to be 114 and 301 nm for D4 and 6, respectively.

The measured adhered wear debris correlates to a wear rates of $6.6 \times 10^{-6} \text{ mm}^3/\text{N} \cdot \text{m}$ and $4.4 \times 10^{-6} \text{ mm}^3/\text{N} \cdot \text{m}$ for D4 and D6, respectively. The reduction in wear rate for D6, which underwent 4 times normal load and over 6 times the lifetime, suggests that the adhesive wear rate is high early on and then diminishes significantly over the course of operating the device. The height has not been measured on D5 because it is still under test or D7 because this device experienced raceway fracture.

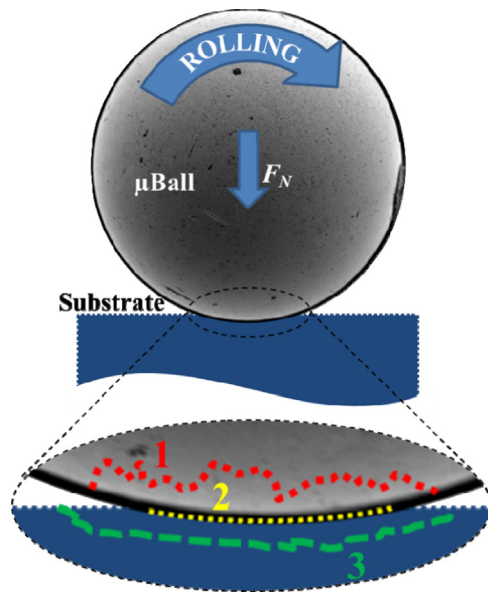


Fig. 10. Schematic of the adhesive wear mechanism. As rolling progresses, new junctions are formed at the ball-substrate interface. This junction will be release by the crack propagation mechanism of the lowest energy, following path 1 through the ball, 2 through the ball-substrate junction, or 3, through the silicon substrate. Stainless steel ball material is observed on thrust-loaded surfaces; therefore, paths 1 and 2 dominate.

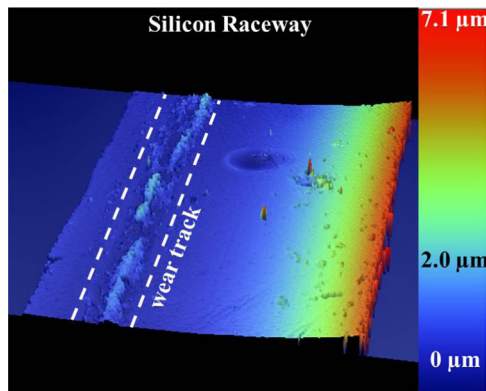


Fig. 11. Optical profile image of silicon raceway with highlighted adhesive wear track.

SEM images in Fig. 12(a–c) shows the adhesion of ball material for D1 and the TiN (D2) and SiC (D3) coated raceways. It should be noted that there is no significant misshaping or observable wear on the balls themselves. This is due to the gradual nature of adhesive wear coupled with the random motion of the ball. Spatially resolved EDS spectra of the wear tracks, in Fig. 12(d–f), reveal adhered ball material on all tested raceways, observed as the presence of chromium and iron peaks in the X-ray spectra.

From the SEM images in Fig. 12(a–c), the specific nature of the ball adhesion can be observed. Ball material adheres non-continuously in the TiN-coated raceway and bare Si raceways. SiC-coated raceways had an approximately continuous coating of the ball material through the wear track of the raceway. The worn ball material exhibited a directionality paralleling the direction of motion of the ball, which suggests some abrasion by the significantly harder film on the steel balls and/or sliding motion in the bearing. The ratio of sliding to rolling contact depends on the ratio of normal to radial load, where higher normal loads will result in increased rolling contact, and the geometry of the system. Increasing radial vibration with decreasing normal load has been observed for these systems previously, supporting this hypothesis [25].

Observation of the adhesive wear patterns from Fig. 12 suggest there is not significant sliding motion for the bare Si raceways but there must be some sliding to cause the sidewall impacts apparent in Fig. 5.

The adhesive wear rate is expected to reach a virtual equilibrium. At equilibrium, the contact path in the raceway has been coated with ball material. The wear, however, does not arrest, it takes place via a ball material transfer. The ball adheres to ball material on the raceway, and fractures in three mechanisms: through the newly formed contact, through the ball (depositing on the raceway), or through the adhered wear track (depositing on the ball). The three mechanisms are equally probable, resulting in a net-zero observed wear rate.

3.2.3. Thin-Film wear

Thin-film coatings tested exhibited wear mechanisms in addition to the adhesive mechanism previously discussed. Inspection revealed surface wear and interfacial delamination observed in both the SEM image (Fig. 12b) and optical micrograph (Fig. 13a) of TiN-coated raceways. The raceway coating remained 60% intact beneath the wear track after 2 M rev., so the delamination is assumed to be a gradual process. The wear was continuous along the ball contact track, with occasional spalling of the coating. The high sub-surface shear stress from the microball contact under load would be expected to induce film delamination, which leads to spalling. SEM inspection revealed that ball material adheres to the TiN film as well as the exposed bare silicon, although there seems to be a significant preference for silicon over TiN surfaces from Fig. 13a. Future TiN coatings with better adhesion properties could serve to mitigate wear in the long term through the lowered affinity for stainless steel adhesion.

The sliding ball motion could have been caused by fragments of the SiC thin film impeding the rolling of the balls, which correlates with the poor performance of the microturbine with SiC thin films shown in Fig. 4. Figs. 12c and 13b show a SiC race after only 30k revolutions of testing at ball contact stress levels less than 100 MPa with significant wear. SiC film wear was limited to the contact area of the ball, while fracturing was observed throughout the raceway (Fig. 13b). The residual stress of the film in the SiC film could have contributed to the rapid wear, although the stress was not measured.

3.2.4. Ball wear

Observation of the wear on the microball provides insight as to the wear mechanisms and general performance of the system. Adhesive wear was the primary mechanism observed on the silicon and coated raceways. Fig. 14 shows a comparison of a fresh ball, and one that has been tested on silicon raceways for 2 M rev. and 20 mN normal load.

The observed wear on the ball, in the form of missing ball material, was minor. The expected depth of removed ball material can be calculated knowing geometries of the system and adhered wear track, assuming all removed ball material adheres to the raceway. The largest adhesive wear track of 301 nm in height and 12 μm in width was observed for device D6, operated for 20 M rev. at 200 mN normal load. This correlates to total wear volume of $1.13 \times 10^{-13} \text{ m}^3$. One hundred, 285-μm-diameter microballs were used for this test, with a calculated total surface area of $2.55 \times 10^{-5} \text{ m}^2$. If it is assumed that the ball randomly and evenly donated material to the raceway surface, then that would result in an overall change in dimension $4.45 \times 10^{-11} \text{ m}$ per ball. This helps to explain why the observed wear on the ball is minimal.

There was also evidence of ball-to-ball contact in the form of minor, directional plow marks. Fig. 15 shows a zoomed in image of a microball bearing exhibiting evidence of the plowing taking place from ball-to-ball contact.

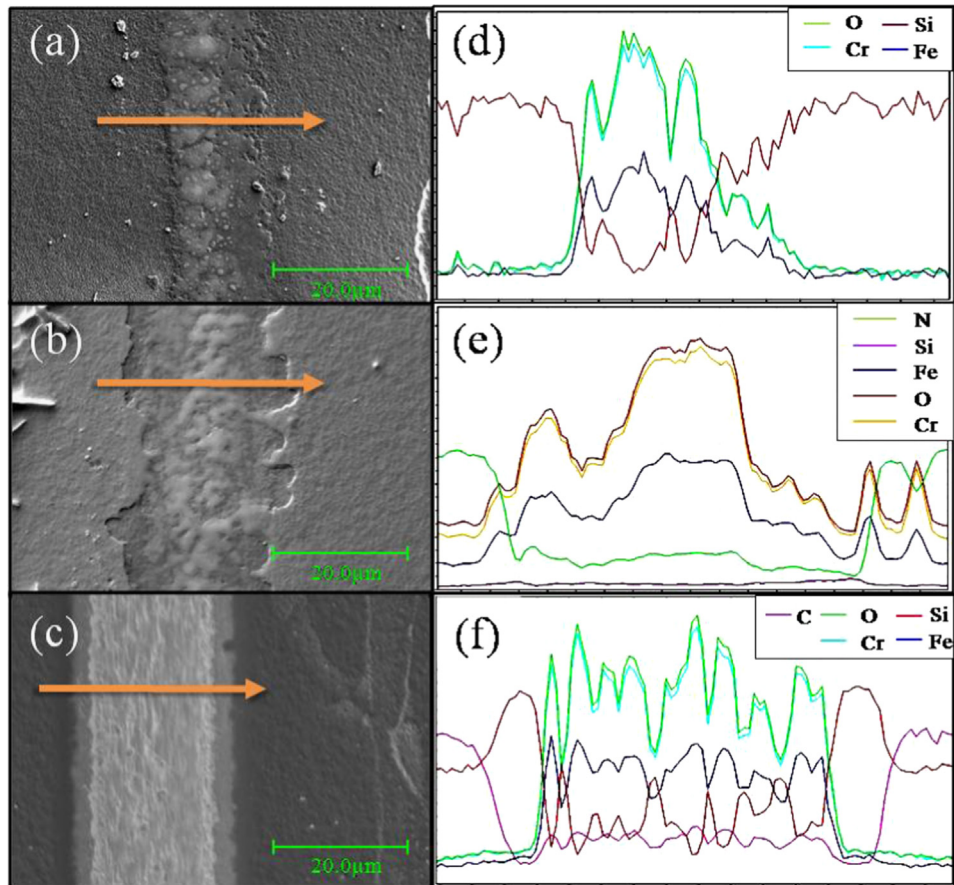


Fig. 12. Left, (a–c) SEM images of characteristic wear track within the ball contact area for (a) silicon, (b) TiN-coated, and (c) SiC-coated raceways. EDS line scans taken perpendicular to each wear track presented in (d–f), correlating with the adjacent SEM image. Iron and chromium are present in each scan, arising from adhered ball material.

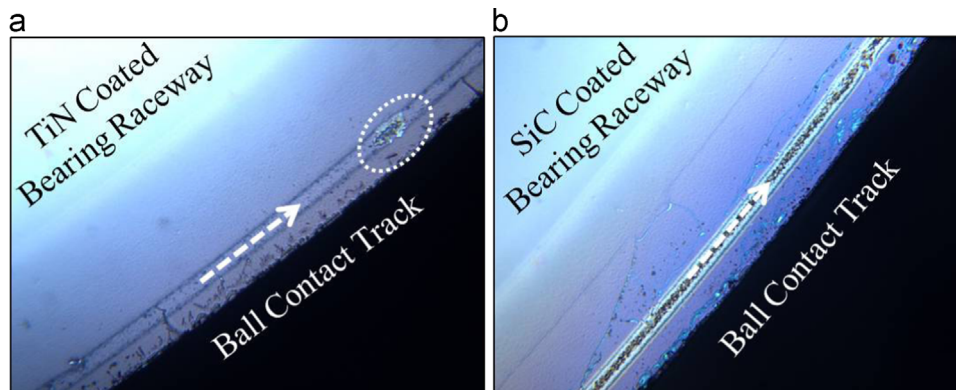


Fig. 13. Optical micrographs of (a) TiN with ball material observed adhered to the bare silicon revealed from thin film wear and (b) SiC-coated raceways exhibiting a continuous track of adhered ball material.

The width of each plow mark is on the order of $1\ \mu\text{m}$, which would suggest the plowing is from ball-to-ball contact, although some skidding could be taking place during start-up of the microturbine when it is operating under very low normal load ($< 5\ \text{mN}$) and likely has significant sliding of the microballs. This skidding at low loads would give a similar wear mechanism.

3.2.5. Raceway fracture

Removal of raceway material was observed in the highest loaded system only, D7 (400 mN rotor load, stress/ball=485 MPa). This wear

regime coincides well with the wear reported within a microfabricated turbopump, operated at similar stresses (518 MPa) [1]. D7 was operated for 8.6 krevs before ultimate failure, attributed to fracture of the raceway. Rolling contact fatigue (RCF) induced spalling caused the progressive removal of raceway surface material, altering the raceway from a flat geometry to a curved surface mimicking the geometry of the ball. Fig. 16 shows an SEM of the worn raceway.

The RCP spalling mechanism in ceramics is described by Wereszczak et al. as the progressive creation of sub-surface cracks within the ceramic, which propagate and coalesce to disconnect a particle from the substrate. The wear process gradually reduces

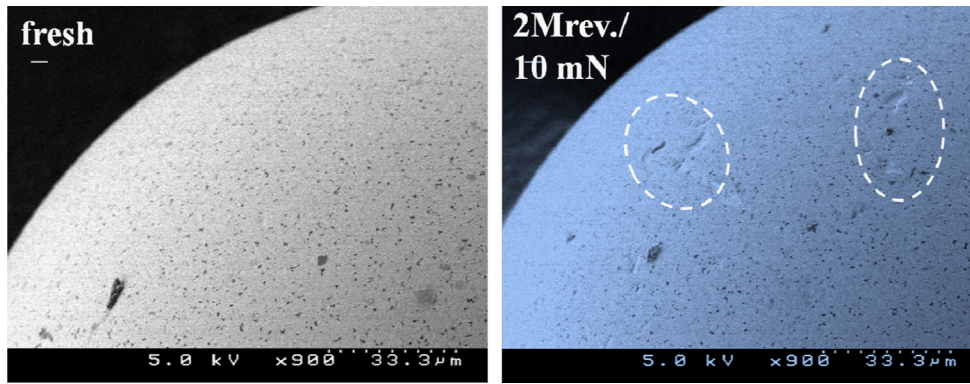


Fig. 14. SEM images of microballs (left) unused microball and (right) microball that was tested in D1. Areas of removed ball material are shown.

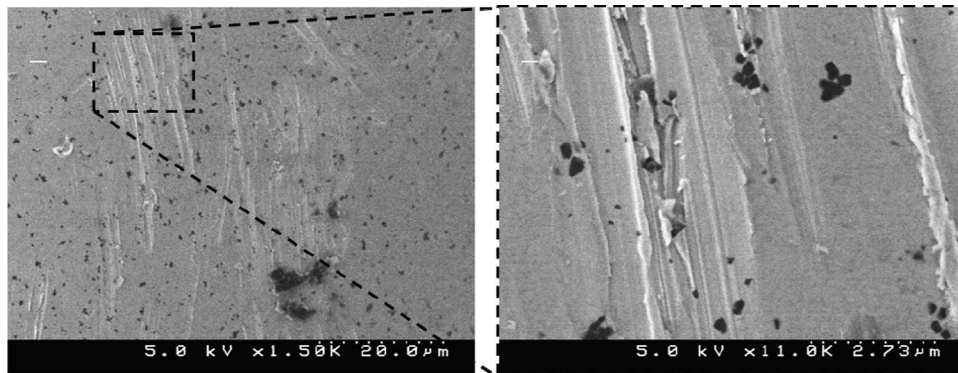


Fig. 15. (left) SEM image of surface of worn microball. (right) zoomed-in image, showing plastic deformation of ball surface.

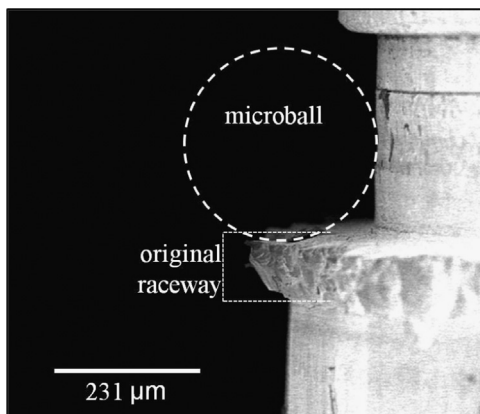


Fig. 16. SEM image of fractured raceway surface of device tested at 400-mN rotor normal loads.

the contact pressure by increasing the contact area. Initial values of mean contact pressure and contact area per ball are calculated from Hertzian contact mechanics to be 485 MPa and $8.0 \mu\text{m}^2$. Upon wear of the raceway, assuming a $150\text{-}\mu\text{m}$ wear groove radius (estimated from Fig. 13), the contact pressure is reduced by one third to 334 MPa due to a 33% increase in contact area to $12.0 \mu\text{m}^2$. The fracture strength of silicon from a tensile test of a micro-fabricated specimen is estimated to be in the range of 1–3 GPa [34], well above the stresses in the bearing; therefore, it is assumed that the spalling is a result of a fatigue mechanism. Bhowmick et al. tested bare silicon samples under static loading and fatigue conditions and found that there is an order of magnitude decrease in strength for cycle lifetimes from 10^3 – 10^6 cycles [35]. This result elucidates the contact pressures that can be used in an engineering application for spall-free operation.

4. Conclusions

The wear mechanisms of a microfabricated ball bearing system are evaluated. A silicon microturbine supported on encapsulated microball bearings was used as the test platform for this study. The raceways were tested bare as well as coated with SiC and TiN thin films to evaluate a possible reduction in friction and wear. Testing was performed by rotating the microturbine rotor under load for a set number of revolutions. Ball material adhesion was found to be the primary wear mechanism, present in both the coated and uncoated raceways. The SiC coating immediately wore, leaving behind a silicon surface that enhanced ball adhesion. The TiN coating wore gradually, lasting 2M rev. before the friction became too erratic to test. Inspection of the raceways revealed that select area of the TiN film had been removed, suggesting a gradual, sub-surface mechanism. For bare silicon raceways, it was shown through Raman spectroscopy that the contact pressure beneath the balls was amorphizing the raceways via a pressure-induced phase change. Silicon raceway fracture dominated over adhesion in only the highest-tested load regime, elucidating the maximum stress allowable for long-term (adhesion regime) operation. The ball strength and chemistry needs to be addressed for microball bearing devices to be operated in the 1 billion revolutions regime. Future work will include the adoption of ceramic balls and the use of surface monolayers to alter the surface chemistries and mitigate adhesion.

Acknowledgment

This work was supported by the U.S. National Science Foundation under award No. 0901411. We would also like to acknowledge

the Maryland Nanocenter and the U.S. Army Research Laboratory Cleanroom Staff.

References

- [1] C.M. Waits, M. McCarthy, R. Ghodssi, A microfabricated spiral-groove turbo-pump supported on microball bearings, *J. Microelectromech. Syst.* 19 (2010) 99–109.
- [2] Y. Naruse, N. Matsubara, K. Mabuchi, M. Izumi, S. Suzuki, Electrostatic micro power generation from low-frequency vibration such as human motion, *J. Micromech. Microeng.* 19 (2009) 094002.
- [3] M. McCarthy, C.M. Waits, M.I. Beyaz, R. Ghodssi, A rotary microactuator supported on encapsulated microball bearings using an electro-pneumatic thrust balance (Sep), *J. Micromech. Microeng.* 19 (2009) 094007.
- [4] N. Ghalichechian, A. Modafe, M.I. Beyaz, R. Ghodssi, Design, fabrication, and characterization of a rotary micromotor supported on microball bearings, *J. Microelectromech. Syst.* 17 (2008) 632–642.
- [5] N. Ghalichechian, A. Modafe, J.H. Lang, R. Ghodssi, Dynamic characterization of a linear electrostatic micromotor supported on microball bearings (16), *Sens. Actuators A-Phys.* 136 (2007) 496–503.
- [6] X.B. Tan, A. Modafe, R. Ghodssi, Measurement and modeling of dynamic rolling friction in linear microball bearings (Dec), *J. Dyn. Syst. Meas. Control-Trans. ASME* 128 (2006) 891–898.
- [7] T.W. Lin, A. Modafe, B. Shapiro, R. Ghodssi, Characterization of dynamic friction in MEMS-Based microball bearings (Jun), *IEEE Trans. Instrum. Meas.* 53 (2004) 839–846.
- [8] M. McCarthy, B. Hanrahan, C. Zorman, R. Ghodssi, Rolling friction in MEMS ball bearings: the effects of loading and solid film lubrication, in: *Proceedings of the STLE/ASME International Joint Tribology Conference*, San Diego, CA, USA, 2007.
- [9] B. Hanrahan, M. McCarthy, J. Balsam, C.M. Waits, H. Bruck, R. Ghodssi, An investigation of hard film coatings for high-speed rotary power MEMS supported in microball bearings, in: *Proceedings of PowerMEMS 2009*, Washington, DC, USA, 2009, pp. 589–592.
- [10] M. McCarthy, C.M. Waits, R. Ghodssi, Dynamic friction and wear in a planar-contact encapsulated microball bearing using an integrated microturbine, *J. Microelectromech. Syst.* 18 (2009) 263–273.
- [11] B. Hanrahan, M. Beyaz, M. McCarthy, C. Waits, and R. Ghodssi, A new performance regime for microfabricated ball bearings, in: *Proceedings of PowerMEMS 2010*, Leuven, Belgium, 2010, pp. 191–194.
- [12] B. Hanrahan, S. Misra, M. Beyaz, J. Feldman, C. Waits, R. Ghodssi, An adhesion-dominated rolling friction regime unique to micro-scale ball bearings, *Tribol. Lett.* (2014).
- [13] W. Weiyuan, W. Yuelin, B. Haifei, X. Bin, B. Minhang, Friction and wear properties in MEMS, *Sens. Actuators A (Physical)* A97–98 (2002) 486–491491.
- [14] D. Asay, M. Dugger, S. Kim, In-situ vapor-phase lubrication of MEMS, *Tribol. Lett.* 29 (2008) 67–74.
- [15] S. Demiri, S. Boedo, L.S. Holsen, Wear characteristics of large aspect ratio silicon microbearing systems, *Wear* 312 (2014) 58–69.
- [16] H. Heshmat, S. Jahanmir, Tribological behavior of ceramics at high sliding speeds in steam (Oct), *Tribol. Lett.* 17 (2004) 359–366.
- [17] S. Achanta, J.P. Celis, On the scale dependence of coefficient of friction in unlubricated sliding contacts, *Wear* 269 (2010) 435–442.
- [18] C.W. Cho, Y.Z. Lee, Tribological characteristics of oxide layer formed on TiN coated silicon wafer (May), *Tribol. Lett.* 16 (2004) 259–263.
- [19] M. Mehregany, S.F. Bart, L.S. Tavrow, J.H. Lang, S.D. Senturia, Principles in design and microfabrication of variable-capacitance side-drive motors, *J. Vacuum Sci. Technol. A-Vacuum Surf. Films* 8 (1990) 3614–3624.
- [20] N.S. Tambe, B. Bhushan, Nanowear mapping: a novel atomic force microscopy based approach for studying nanoscale wear at high sliding velocities (Sep), *Tribol. Lett.* 20 (2005) 83–90.
- [21] I.S.Y. Ku, T. Reddyhoff, A.S. Holmes, H.A. Spikes, Wear of silicon surfaces in MEMS, *Wear* 271 (2011) 1050–1058.
- [22] M. Alberts, K. Kalaitzidou, S. Melkote, An investigation of graphite nanoplatelets as lubricant in grinding, *Int. J. Mach. Tools Manuf.* 49 (2009) 966–970.
- [23] M.R. Hampson, E.W. Roberts, M.D. Cropper, R.B. Watters, D.J. Forster, Towards the effective solid lubrication of ball bearings operating at high temperature, *Proc. Inst. Mech. Eng. Part J-J. Eng. Tribol.* 222 (2008) 1041–1049.
- [24] R. Bandorf, D.M. Paulkowski, K.I. Schifffmann, R.L.A. Kuster, Tribological improvement of moving microparts by application of thin films and micro-patterning (Sep), *J. Phys. Condens. Matter* 20 (2008).
- [25] B. Hanrahan, J. Feldman, S. Misra, P.D. Mitcheson, C. Waits, R. Ghodssi, Off-The-Shelf MEMS For Rotary MEMS, in: *Proceedings of the International Conference on MicroElectroMechanical Systems*, Paris, France, 2012, pp. 579–582.
- [26] B. Hanrahan, *Tribology of Microball Bearing MEMS (Doctor of Philosophy)*, Materials Science and Engineering, University of Maryland, 2013.
- [27] N. Kumar, S. Dash, S. Rajagopalan, A. Bahuguna, A.K. Tyagi, B. Raj, Tribological properties of SiC coatings deposited by r.f. magnetron sputtering as a function of substrate temperature, *Philos. Mag. Lett.* 91 (2011) 465–472.
- [28] V. Chawla, R. Jayaganthan, R. Chandra, Structural characterizations of magnetron sputtered nanocrystalline TiN thin films, *Mater. Charact.* 59 (2008) 1015.
- [29] T. Juliano, V. Domnich, Y. Gogotsi, Examining pressure-induced phase transformations in silicon by spherical indentation and Raman spectroscopy: a statistical study (Oct), *J. Mater. Res.* 19 (2004) 3099–3108.
- [30] F. Demangeot, P. Puech, V. Paillard, V. Domnich, Y.G. Gogotsi, Spatial distribution of strain and phases in Si nano-indentation analysed by Raman mapping, in: *Zurich-Uetikon (Ed.), Gettering and Defect Engineering in Semiconductor Technology*, 82–84, Trans Tech Publications Ltd, 2002, pp. 777–782.
- [31] V. Domnich, Y. Gogotsi, S. Dub, Effect of phase transformations on the shape of the unloading curve in the nanoindentation of silicon, *Appl. Phys. Lett.* 76 (2000) 2214–2216.
- [32] D.M. Follstaedt, J.A. Knapp, S.M. Myers, Mechanical properties of ion-implanted amorphous silicon, *J. Mater. Res.* 19 (2004) 338–346.
- [33] J.G. Swadener, M. Nastasi, Increasing the fracture toughness of silicon by ion implantation, *Nuclear Instrum. Methods Phys. Res. Sect. B-Beam Interact. Mater. Atoms* 206 (2003) 937–940.
- [34] M.S. Gaither, F.W. DelRio, R.S. Gates, E.R. Fuller, R.F. Cook, Strength distribution of single-crystal silicon theta-like specimens (Aug), *Scr. Mater.* 63 (2010) 422–425.
- [35] S. Bhowmick, J.J. Melendez-Martinez, B.R. Lawn, Contact fatigue of silicon, *J. Mater. Res.* 23 (2008) 1175–1184.